

# ML-Powered FPGA-based Real-Time Quantum State Discrimination Enabling Mid-circuit Measurements

Neel R. Vora<sup>1,2</sup>, Yilun Xu<sup>1,\*</sup>, Akel Hashim<sup>3</sup>, Neelay Fruitwala<sup>1</sup>, Ho Nam Nguyen<sup>3</sup>,  
Haoran Liao<sup>3</sup>, Jan Balewski<sup>1</sup>, Abhi Rajagopala<sup>1</sup>, Kasra Nowrouzi<sup>1</sup>, Qing Ji<sup>1</sup>,  
K. Birgitta Whaley<sup>3</sup>, Irfan Siddiqi<sup>3</sup>, Phuc Nguyen<sup>2,\*</sup>, Gang Huang<sup>1</sup>

<sup>1</sup>Lawrence Berkeley National Laboratory,

<sup>2</sup>University of Massachusetts Amherst,

<sup>3</sup>University of California, Berkeley

\*Co-corresponding authors: Yilun Xu (yilunxu@lbl.gov) and Phuc Nguyen (vp.nguyen@cs.umass.edu)

## ABSTRACT

Similar to reading the transistor state in classical computers, identifying the quantum bit (qubit) state is a fundamental operation to translate quantum information. However, identifying the qubit state has been the slowest and most susceptible to errors operation on superconducting quantum processors. Most existing qubit state discriminating algorithms have only been implemented and optimized “after the fact”—using offline data transferred from a quantum control circuit to host computers. Real-time state discrimination is not possible because a superconducting qubit state only survives for a few hundred  $\mu\text{s}$ , which is much shorter than the communication delay between the readout circuit and the host computer (i.e., tens of  $\text{ms}$ ).

Mid-circuit measurement, where measurements are conducted on qubits at intermediate stages within a quantum circuit rather than solely at the end, represents an advanced technique for qubit reuse in quantum computing. This approach expands the computational toolkit, enabling the implementation of more sophisticated error correction algorithms and maximizing the potential of the noisy intermediate-scale quantum (NISQ) era devices available today. For mid-circuit measurements necessitating single-shot readout, it is imperative to employ an in-situ technique for state discrimination characterized by low latency and high accuracy.

This paper introduces *QubiCML*, a field-programmable gate array (FPGA) based system for real-time qubit state discrimination enabling mid-circuit measurement—the ability to measure the qubit state at the electronic control circuit before/without transferring quantum data to a host computer. *QubiCML* provides in-situ real-time feedback and verification for quantum algorithm development and optimization. A multi-layer neural network has been designed and deployed on the FPGA platform to ensure accurate in-situ state discrimination. For the first time, ML-powered quantum state discrimination has been implemented on a radio frequency system-on-chip (RFSoc) FPGA platform (Xilinx ZCU216). The deployed lightweight network on the FPGA hardware

only takes 54 ns to complete each inference (state measurement). We evaluated *QubiCML*’s performance on in-house superconducting quantum processors and obtained an average accuracy of 98.5% with only 500 ns readout length. *QubiCML* has the potential to become the standard real-time state discrimination method for the quantum community.

## 1 INTRODUCTION

Quantum computing is a rapidly evolving technology that holds the promise of revolutionizing computation across various domains thanks to its ability to solve specific classes of complex problems. Quantum computers have strong computational advantages compared to classical computers for certain problems as they leverage the quantum-mechanical properties of quantum bits (qubits). In the current practice, qubit information is manipulated by an electronic control system, which includes qubit readout and control pipelines, to orchestrate the execution of quantum programs. The control pipeline transmits precise gate pulses to qubits while the readout pipeline measures the qubits’ states. Control and readout operations can be executed on hundreds of qubits [3], while a fully utilized 50-100 qubits quantum computer may be able to perform tasks that surpass the capabilities of today’s classical digital computers [33].

Among many advanced qubits architectures introduced recently [10, 21], superconducting qubits [21] have emerged as the leading quantum computing platform in the past two decades. Superconducting qubit information can be obtained by state measurement [22], a process to identify the qubit state. However, this is the slowest operation in quantum computing. While individual superconducting qubit supports around 100  $\mu\text{s}$  coherence time (i.e., time to hold the information), the delay in streaming data from the readout measurement circuit to the host computer for state discrimination falls within the millisecond ( $\text{ms}$ ) range. Hence, real-time state measurement is not possible. In the current practice, the measurement must be done at the end of the circuit, which is normally a classical host computer. The

state discrimination results are computed on a classical computer [12, 16, 25], where it is then subjected to classical post-processing. When performing multiple state discrimination for computing tasks, the measurements are queued up for execution, demanding computationally expensive resources, and hindering scalability.

Mid-circuit measurement stands out as the most promising approach to maximize the potential of the NISQ-era devices available today, and address the scalability issue [1, 39]. Mid-circuit measurement reuses qubits, thereby minimizing the number of required qubits, condensing larger circuits for operation on smaller devices, and enabling more sophisticated error correction algorithms. The key idea of mid-circuit measurements is to introduce classical logic, i.e., FPGA, next to quantum processors. The classical mid-processing of the quantum systems is now extended with additional hardware and control systems to perform mid-circuit measurements during the runtime of one circuit. A measurement is taken as it has always been taken, but the circuit does not need to be terminated. Classical logic is applied in situ, and the process continues seamlessly. This approach would reduce the time qubits needed to maintain coherence by allowing earlier measurement and initialization, minimize decoherence by measuring qubits promptly, enable real-time error detection and correction, facilitate state evolution with conditional operations without unwanted entanglement, and replace certain quantum operations with classical logic to simplify circuits [19]. Additionally, it allows for the adjustment of parameters in variational quantum algorithms directly on the quantum processor, saving time and the possibility to measure, reset, and reuse qubits, which is crucial given the current scarcity of qubits. For mid-circuit measurements, necessitating single-shot readout, an in situ technique for state discrimination with low latency and high accuracy is required. *However, there is no real-time in situ intelligence discrimination for mid-circuit measurement nowadays!*

In parallel, qubit readout is among the operations most susceptible to errors in state-of-the-art superconducting quantum processors. Errors arise during all stages of the circuit model that are used to retrieve quantum information [13]. State-of-the-art IBM quantum computer has readout error rates ranging from 0.1% for some qubits to >10% for other qubits [2, 29]. Multiple error sources have been identified, including relaxation errors (generated during relaxation phase after qubits excited from the ground state) [32], crosstalk errors (reading multiple qubits at the same time using the frequency-multiplexed method) [24], excitation errors (similar to relaxation errors but occur when the readout pulses excite a qubit) [40], and environmental noises [27, 30, 37, 42]. Artificial intelligence (AI) / machine learning (ML) techniques have been actively leveraged to address these issues.

For example, Satvik et al. confirm the feasibility of designing an FPGA-friendly ML algorithm to improve 16.4% of accuracy for single qubit measurements [29]. In another example, Benjamin Lienhard et al. present a deep neural network (DNN) that significantly reduces crosstalk error while simultaneously performing in-state discrimination of up to 5 qubits using a single readout circuit [24]. *However, none of the current ML algorithms for state discrimination have been implemented in mid-circuit hardware!*

These observations raise a fundamental question in quantum computing system research:

Can we design and implement a real-time and in-situ ML-powered system for mid-circuit measurements?

The answer to this question is far from obvious massive engineering effort. Besides the noises discussed in the literature, the impact of system design on the readout accuracy is understudied. While there are strong similarities between radio frequency (RF) systems that have been discussed extensively, it is unclear if our many years of knowledge in RF research can be leveraged to advance quantum computing circuits. Moreover, as readout, analog-to-digital converter (ADC) samples at an extremely fast rate (i.e., Giga-samples per second (GSPS)), processing and computing such a high data rate is extremely difficult. Lastly, developing a machine learning model that is able to perform training and real-time inference on qubit data on the hardware faces many challenges from modeling to implementation.

This paper addresses the aforementioned challenges and makes the following technical contributions.

- We analyze the current limitations of existing quantum stage classification in superconducting qubit research and derive an algorithm from adjusting the multiplexing signal through digital local oscillator (DLO) optimization to optimize signal fidelity.
- We characterize the current readout pulse design and study a novel approach to obtain optimized readout pulses that significantly boost the accuracy of qubit state discrimination.
- We derive a machine learning model to obtain 98.5% readout fidelity with even a short readout pulse of 500 ns of quantum data. Note that 500 ns readout is considered state-of-the-art, which was also obtained by leading teams such as Google [6] and IBM [11].
- We study and design a neural network structure that runs on an FPGA platform to finish its inference task within 54 ns. **This is the first system to support real-time ML state discrimination for mid-circuit measurement.**

- We evaluate the proposed system using three superconducting transmon qubits and confirm the system’s feasibility, robustness, and scalability.

We introduce *QubiCML*, an FPGA-based ML-accelerated system for real-time qubit state discrimination for mid-circuit measurement in quantum computing.

The remainder of this paper is structured as follows. Sec. 2 describes the fundamentals of qubit readout architecture and their limitations. Sec. 3 highlights *QubiCML*’s overview. Sec. 4 explains the processes to optimize the readout and control. Sec. 5-6 details the FPGA-based ML technique for state discrimination. We discuss the evaluation of *QubiCML*, related works, and conclude the paper in Secs. 7-9.

## 2 FUNDAMENTALS OF QUBIT CONTROL AND READOUT

This section describes the principle of qubit readouts, the current architecture, and its limitations.

**Principle of qubit readout.** In quantum computing, a qubit, like a classical bit, represents basic information. Unlike classical bits, qubits can be 0 and 1 simultaneously due to superposition, expressed as  $|\psi\rangle = \alpha|0\rangle + \beta|1\rangle$ , where  $\alpha$  and  $\beta$  are complex probability amplitudes. Upon measurement, a qubit collapses to either state 0 or 1 according to these probabilities. This property enables quantum computers to outperform classical ones in certain calculations. Readout refers to the process of determining the state of a qubit. After a measurement, the qubit is typically in the ground state (‘0’) or excited state (‘1’). Precise measurements are crucial for accurately characterizing qubit states, as they enable researchers to understand and control quantum systems effectively. For example, precise measurements are essential for tasks like error correction and quantum state manipulation. Real-time measurements are essential for enabling closed-loop control in quantum systems, particularly for error correction research. Real-time feedback allows researchers to make rapid adjustments to the system based on current measurements, improving system stability and performance.

**Qubit control and readout architecture.** An example common schematic of a superconducting qubit control and readout is illustrated in Figure 1. In particular, the control and readout pulses, generated by an RFSoc or arbitrary waveform generator (AWG), are sent through attenuated signal lines to the readout resonator on the quantum processing unit (QPU). The transmitted readout signal is amplified by a traveling-wave parametric amplifier (TWPA), a high-electron-mobility transistor (HEMT), and room-temperature amplifiers at different stages. Afterward, the signal is directed to an ADC for sampling, and then to an FPGA for digital processing. This schematic is often implemented by dedicated systems (e.g., Zurich Instruments [5], Keysight [4]) or FPGA platforms (e.g., QubiC [43, 44]).

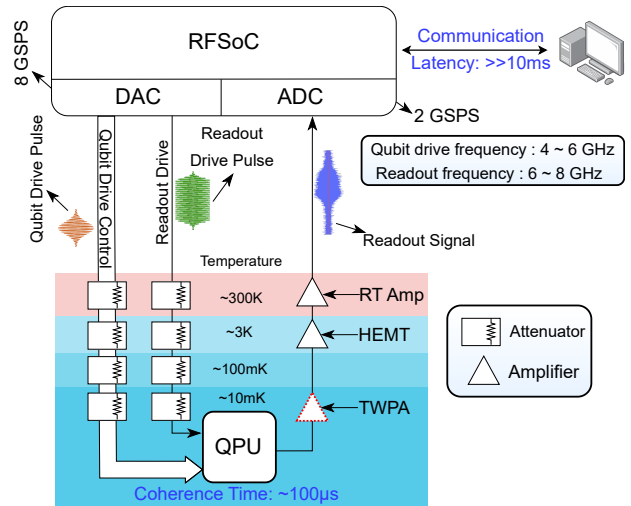


**Figure 1: Schematic of common superconducting transmon qubit control and readout.**

**Delays and errors in quantum readouts.** From Figure 1, multiple problems must be addressed in order to build robust and usable control system. Obviously, the inconsistency between the coherence time of the qubits and the delay of data processing is one of the major issues. However, solving this issue requires a holistic approach to rethink both the hardware and software architecture of the control system.

Additionally, multiple error sources of qubit readouts have been identified in the literature. Relaxation errors arise from qubits relaxing after being excited from the ground state [32]. Similarly, crosstalk errors, resulting from the simultaneous reading of multiple qubits through frequency-multiplexed methods, pose a challenge to scale up the number of qubits that can be supported at the same time [24]. Excitation errors, akin to relaxation errors but occurring when readout pulses inadvertently excite a qubit, further complicate the fidelity of quantum operations [40]. Moreover, environmental noises contribute to the overall error landscape in quantum systems, further necessitating robust error correction strategies [27, 30, 37]. Characterizing and mitigating these errors are ongoing research efforts.

## 3 QUBICML SYSTEM

In this section, we present *QubiCML*, an FPGA-based platform for real-time qubit state discrimination for mid-circuit measurements. *QubiCML* learns the trajectory of the qubit states through its closed-loop and optimized architecture to accurately differentiate qubit states reliably in real-time.

**Basic hardware and software:** *QubiCML* leverages QubiC 2.0 readout hardware [43, 44] as the base implementation. Compared to other commercial systems such as Zurich Instruments [5] or Keysight [4], QubiC is a more flexible platform, which allows researchers/developers to modify/upgrade

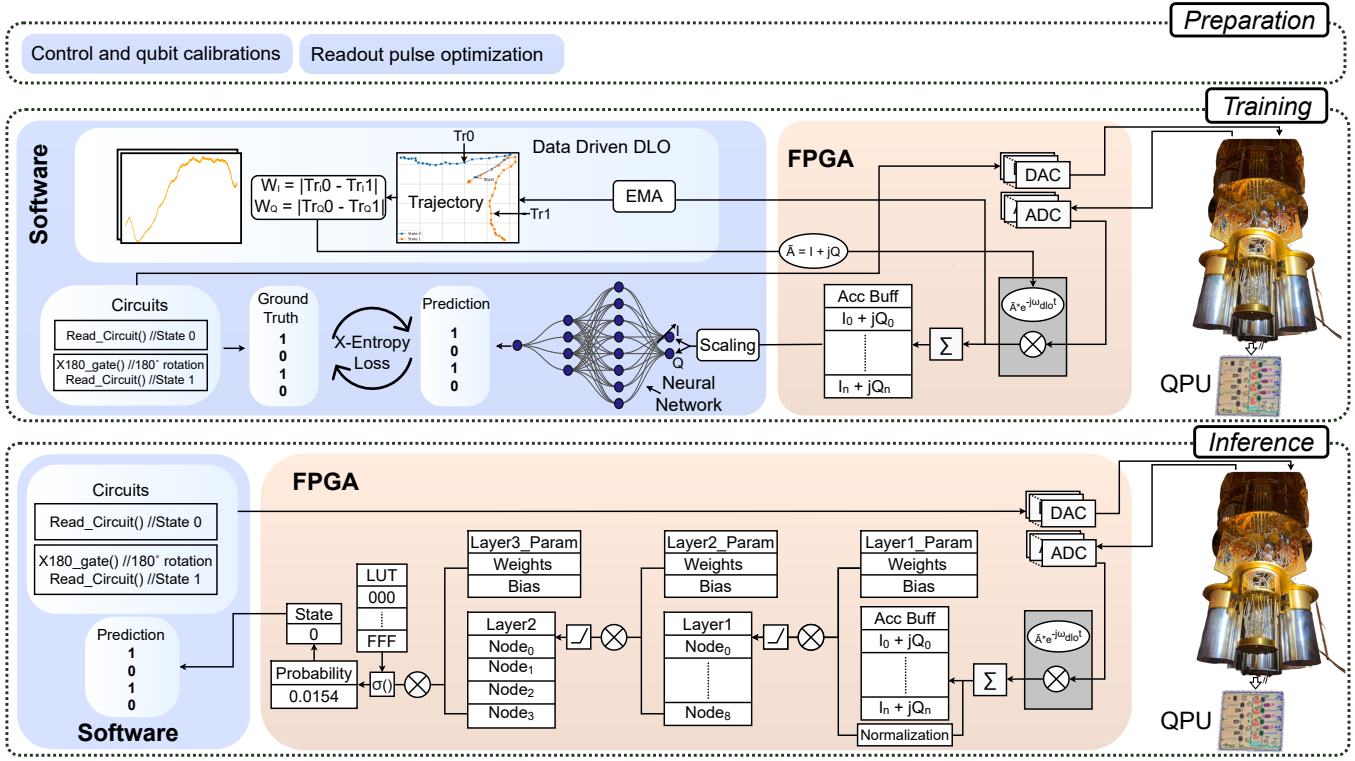


Figure 2: The overview architecture of QubiCML.

all of its hardware and software components. QubiC 2.0 includes digital-to-analog converters (DAC) to generate RF pulses for qubit manipulation, an ADC to measure the qubit response, and additional digital mixing component leveraging a digital local oscillator to provide I/Q data, which are then streamed to the host computer, all are implemented on Zynq UltraScale+.

Three main phases in QubiCML’s operation include: (1) Preparation, (2) Training, and (3) Inference (Figure 2).

**Preparation:** To prepare for the measurement, the qubit must be calibrated thoroughly. The calibrated parameters will be stored in a calibration file, which is then shared among the qubits users. While it sounds like an expensive overhead, this is a common step/limitation of current superconducting qubit technology. Besides this, we also found that the hardware inconsistency and imperfection might also affect the state discrimination accuracy and discovered one potential approach to further improve the reliability of the qubit by optimizing the readout pulse structure (Sec. 4.1).

**Training:** This step includes optimizing DLO and training the machine learning model for qubit state discrimination. First, we explore a data-driven method to optimize the envelope structure when mixing ADC’s raw signal with DLO (Sec 4.2). After calibrating the qubits and optimizing DLO,

we initiate data collection to train the ML model by configuring circuits to perform various operations, allowing qubits to assume either of two states. Next, we construct a machine-learning model to perform state discrimination on accumulated qubit data of 50,000 readout samples (shots) (with IQ component), for each state (Sec.5).

Since the states are predetermined during circuit creation, they serve as ground truth labels for the ML model. The range of accumulated data could be from  $(-2^{31})$  to  $(2^{31} - 1)$ . This large value could lead to saturation when we implement ML on FPGA [31], which makes scaling of these accumulated data an important process (Sec 6.2). We use scaled data as input to the ML model, utilizing feed-forward neural network (FNN) [9] that takes two inputs, i.e. scaled I and Q components (Sec 5), and the output of the network will be the actual state of the input shot. The network is trained until its parameters are tuned to perform qubit state discrimination with high fidelity.

**On-chip inference:** After training the model, we deploy it on FPGA for multi-qubit real-time inference. This integration process begins by converting the parameter format from floating point to fixed point notation (Sec 6.1) since the former requires additional resources [36]. Then, we study and modify the normalization procedure to remove division

operation (Sec 6.2) because performing division on FPGA is resource-expensive [28].

Following these modifications, we implement a forward pass of the neural network on the FPGA. This primarily consists of a series of summation and multiplication operations, followed by an activation layer. These operations are executed serially across the different layers. Once the final layer, which typically involves a sigmoid activation, completes all its operations, we obtain the discrimination result from the ML model. This entire process just takes  $54ns$  (Sec 6.3). Our system also allows loading model parameters from block random-access memory (RAM), ensuring scalability across various qubits with different frequencies. This feature facilitates the seamless integration of models, enhancing adaptability to diverse experimental setups.

## 4 READOUT & CONTROL OPTIMIZATION

This step prepares the *QubiCML* to ensure its design and parameters are optimized for state discrimination. Two consecutive optimizations are performed to (1) optimize the readout RF pulses for identifying the maximum information from the readout data and (2) interactively adapt the DLO signal pulses to increase the Mahalanobis distance [34] between quantum state clusters, further boosting the accuracy of state discrimination.

### 4.1 Optimizing RF pulses

RF pulses for controlling and measuring superconducting qubits are typically amplitude-modulated signals with defined frequency, phase, and envelope. Similar to optimizing high-frequency waveforms for radar/wireless communication systems, the non-linearity of hardware components might also contribute to the fidelity of the measured data. This means the structure of the pulses is unknown and can be used to optimize the readout accuracy. We explored multiple waveforms and found that besides frequency and phase, the envelope of the transmitted pulses has a direct relationship with the ability to extract information from qubits. In other words, the waveform of the readout can be optimized through an iterative process with the objective is maximizing Hamiltonian distance between qubit states.

Traditionally, a cosine-edge square wave with a ramping of 0.25% is used as the envelope for RF pulses [43]. However, due to its slow-rising edge, efficient information capture from the beginning of the qubit signal is hindered, thereby limiting readout time optimization. We explored multiple waveform designs for the pulses and found that by increasing the steepness of the rising and falling edges of the cosine-edge square wave, the Mahalanobis distance significantly increased, as illustrated in Figure 3. This adjustment enables efficient information capture from beginning of the qubit

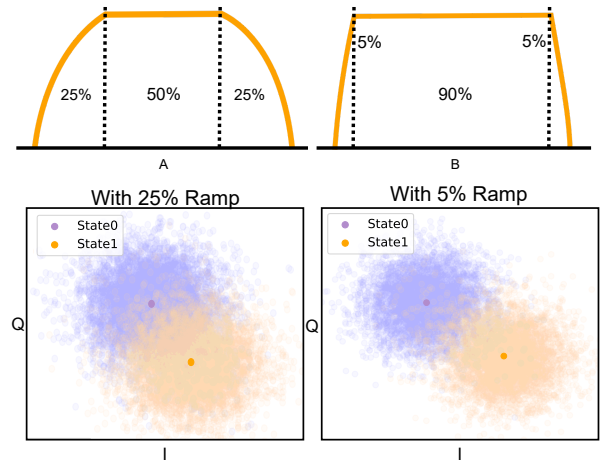


Figure 3: Impact of readout pulse optimization

signal while avoiding signal saturation. Through a series of experiments, we determined that using a cosine edge with ramping between 0.07% and 0.02% significantly reduces readout time while maintaining accuracy, as shown in the Table below. Note that these quantum computing processors do not include TWPA [27]. With TWPA, pulse readout can be reduced to a few hundred nanoseconds, as discussed in later sections.

Readout Time	Ramp 25%	Ramp 5%
$2\mu s$	95.73%	97.64%
$1.5\mu s$	91.66%	95.57%
$1\mu s$	85.02%	91.50%

Table 1: Average fidelity obtained from readout pulse optimization

**Finding:** Ramping edge design of readout pulse has a significant effect on the state discriminator result.

### 4.2 Optimizing DLO signal

A complex DLO with frequency and phase matching that of the readout signal and with a ADC sampling rate is utilized for mixing with the readout signal from the ADC ( $ADC_{raw}$ ) (Eq. 1), where  $ADC_{mixed}$  is the mixed signal with frequency  $\omega_{dlo}$ . This yields the In-phase (I) and Quadrature (Q) components of the qubit readout signal as the real and imaginary components, respectively.

$$ADC_{mixed} = e^{-j\omega_{dlo}t} \cdot ADC_{raw} \quad | \quad \omega_{dlo} = 2\pi f_{dlo}; \quad (1)$$

In the current practice, most of the control systems employ a *standard square wave* as the envelope for the DLO function, treating each sample uniformly over time. However, our empirical analysis shows that this approach did not accurately reflect the true significance of each sample. In fact, it became apparent that not all samples contributed

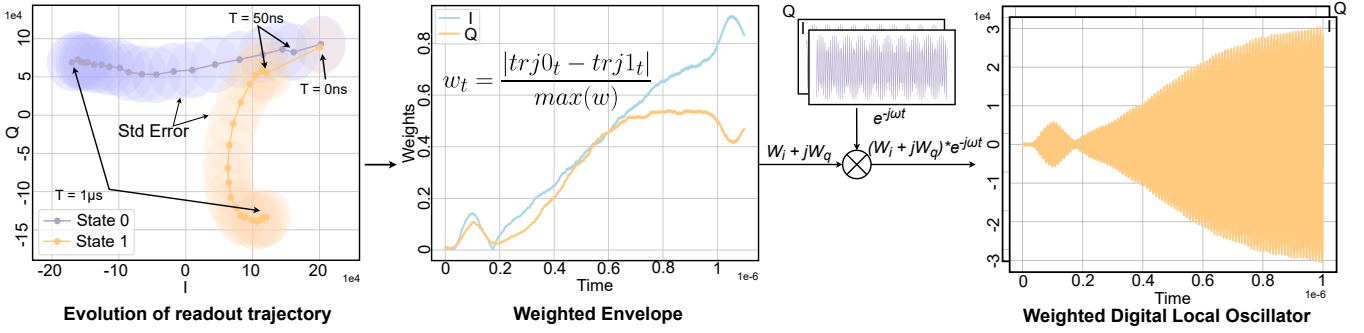


**Figure 4: The overview of the proposed data-driven DLO optimization approach where weighted envelope (middle figure) is used instead of the standard square wave in current practice.**

equally to state discrimination, and this phenomenon had been reported [35, 41], but little attention has been paid.

Thus, assuming that there exists a "perfect" weighted DLO signal—which takes into account the non-linearity and imperfection of the hardware circuit and ADC to generate a stronger discriminated qubit state from the data, the mixed ADC equation can be rewritten as follows:

$$WADC_{mixed} = W \cdot e^{-j\omega_{dlo}t} \cdot ADC, \quad (2)$$

where  $W \cdot e^{-j\omega_{dlo}t}$  is the optimized DLO envelop structure. The question now is how to calculate the weight vector  $W$ . One possible solution is to leverage the data collected to obtain the optimized DLO signal structure. To do so, we collect 10K  $ADC_{mixed}$  (labeled) shots mixed with normal DLO for both ground and excited states. Then we perform exponential moving average (EMA) [18] on  $ADC_{mixed}$  and get  $ADC_{ema}$  with  $\alpha = 0.01$  using Eq. 3. This helps identify sample instances more accurately while avoiding sudden deviation from the trajectory.

$$\begin{aligned} adc_{ema}^t &= (adc_{mixed}^t \cdot \alpha) + adc_{ema}^{t-1} \cdot (1 - \alpha) \\ adc_{ema}^t &\in ADC_{ema}; \\ State0 &= ADC_{ema} \in \text{ground state} \\ State1 &= ADC_{ema} \in \text{excited state} \end{aligned} \quad (3)$$

As shown in Figure 4 (a), we then split the ground state and excited state trajectory (states are pre-determined while preparing the circuits) and get the mean trajectory across the given state as per Eq. 4.

$$trj0_t = \frac{1}{n} \sum_{i=0}^n State0_i^t; \quad trj1_t = \frac{1}{m} \sum_{i=0}^m State1_i^t \quad (4)$$

We use this complex  $trj0$  and  $trj1$  to calculate the weights vector  $W$  (Figure 4b). This complex weights vector is multiplied with DLO carrier to get weighted DLO (Figure 4c). This weighted DLO is then mixed with qubit readout signals that gives  $WADC_{mixed}$ , which is the same as doing weighted sum over  $ADC_{mixed}$ , i.e.  $\sum_{t=0}^{t=T} WADC_{mixed} = \sum_{t=0}^{t=T} w_t(I_t + jQ_t)$ .

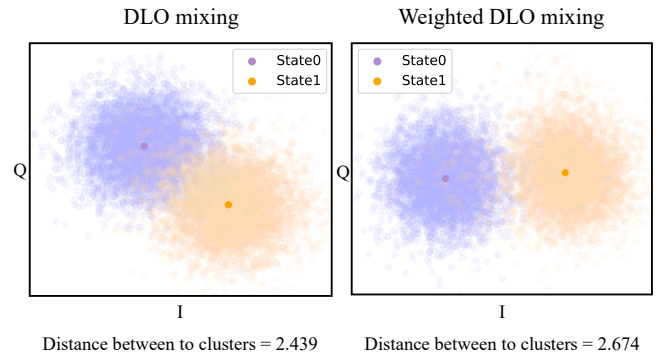


**Figure 5: Impact of weighted DLO based optimization. Distance is calculated using Mahalanobis formula.**

The above strategy effectively enhances the distinction between the accumulated sum of  $ADC_{mixed}$  signals corresponding to the ground state and excited state, as depicted in Figure 5. This approach also significantly reduces the required readout time while preserving the high fidelity of state discrimination. Table 2 quantifies the average impact of DLO optimization, revealing a notable 1.92% increase in fidelity for a  $1\mu s$  readout duration. By combining this optimization technique with pulse optimization (Sec. 4.1), we observed a substantial 25% reduction in the readout time requirement for the TWPA-less setup, compared to the baseline configuration without any readout or DLO optimization.

Readout Time	Baseline	Readout + DLO optimization
$2\mu s$	95.73%	97.81%
$1.5\mu s$	91.66%	97.49%
$1\mu s$	85.02%	93.17%

**Table 2: Average fidelity impact from data-driven DLO and readout pulse optimization**

**Finding:** DLO signal can be optimized using a data-driven approach to enhance the accuracy of state discrimination.

## 5 ML-ACCELERATED QUBIT STATE DISCRIMINATION

Accurate identification of qubit states is crucial in quantum computing, enabling tasks like state preparation and error correction, which are essential for achieving quantum computational supremacy [8, 15]. The conventional approach to qubit state discrimination involves transmitting data from the accumulated buffer, denoted as  $ACC_{buff}$ , to the host computer/software. Subsequently, a pre-trained Gaussian Mixture Model (GMM) based classifier is employed to discern the qubit’s state [43]. However, this method is plagued by a significant issue of latency. Even with high-bandwidth Ethernet connections, the process typically takes several milliseconds before discrimination results are obtained. In quantum computing, such latency represents a substantial delay for systems aiming to provide real-time feedback based on qubit discrimination.

In this project, we employed a feed-forward neural networks (FNN) based binary classifier on FPGA to achieve real-time state discrimination. Initially, we gathered 50,000 shots (heralding pulse to exclude outliers) for both ground and excited states, where each shot, denoted as  $ADC_{acc}$ , represented a complex number with the real component as  $I$  and the imaginary component as  $Q$ . The entire dataset underwent shifting to center the mean at  $[0,0]$ , followed by normalization to scale down the data within the range of 0-1. This scaling step is crucial before feeding the data into neural networks for further processing [38]. We adopted min-max normalization for this purpose (Sec 6.2).

The normalized data served as the input for training the neural network. Our FNN architecture comprised an input layer with two nodes, two hidden layers with 8 and 4 nodes, respectively, and an output layer with one node. In total, we had 65 trainable parameters, including 52 weights and 13 biases. Each hidden layer was followed by a rectified linear unit (ReLU) activation [14], and the final layer employed a sigmoid activation [23] unit to output the state of the qubit.

For training, the network was initialized with random weights and biases. We partitioned the 100,000 normalized data sets (ground and excited states) and the pre-determined ground truth labels into a training set of 60,000 and a testing set of 40,000. The training set was further divided into batches of 64 sets. Each batch, sized  $[64 \times 2]$  (Batch size  $\times$  I, Q), underwent a forward pass through the network, yielding probabilities from the final activation unit. These outputs, along with the ground truth label, were used to calculate the

network’s loss/divergence, employing binary cross-entropy as the loss function [45]. The gradients of this loss were then back-propagated through the network using ADAM optimization [20]. This process was repeated for all batches of the training set over 100 epochs or until the loss converged.

During experimentation, we subjected the model, trained specifically for its corresponding qubits, to a new series of tests before integrating it on FPGA. Our findings revealed a notable 1% improvement in fidelity solely attributable to DLO readout optimization. Furthermore, when compared to the baseline configuration, we observed a substantial 6% enhancement in fidelity for a  $1.5\mu s$  readout duration (without TWPA). Similar results are obtained with shorter pulses of  $500ns$  (with TWPA). These results underscore the efficacy of our optimization strategies in achieving significant improvements in qubit state discrimination fidelity (Table 3).

Readout Time	Baseline	QubiCML
$2\mu s$	95.73%	98.56%
$1.5\mu s$	91.66%	98.32%
$1\mu s$	85.02%	94.33%

**Table 3: Average fidelity from QubiCML without TWPA**

**Finding:** Neural network is able to discriminate the qubit state even with a short pulse while maintaining high fidelity.

## 6 ON-CHIP SYSTEM FOR QUBIT STATE DISCRIMINATION

We leverage FPGA for qubit discrimination due to its ability to perform parallel processing and real-time computations. The overview of the proposed pipeline is depicted in Figure 6. FPGA offers low-latency processing, which is crucial for achieving real-time feedback, especially for tasks like mid-circuit measurements. However, the trained ML models cannot be directly deployed on FPGA hardware. Further investigations on (1) data representation, (2) bit width manipulation, and (3) normalization must be devoted.

### 6.1 Data notation on FPGA

In traditional software-based neural networks, parameters and input data are typically represented using floating-point notation, often in float 32-bit format. However, translating floating-point notation to FPGA poses challenges, requiring additional resources for each operation. Therefore, we opt to convert all parameters and input data to fixed-point notation facilitating FPGA processing. The bit width of these parameters and input is determined based on the types of operations required and the resources available for executing

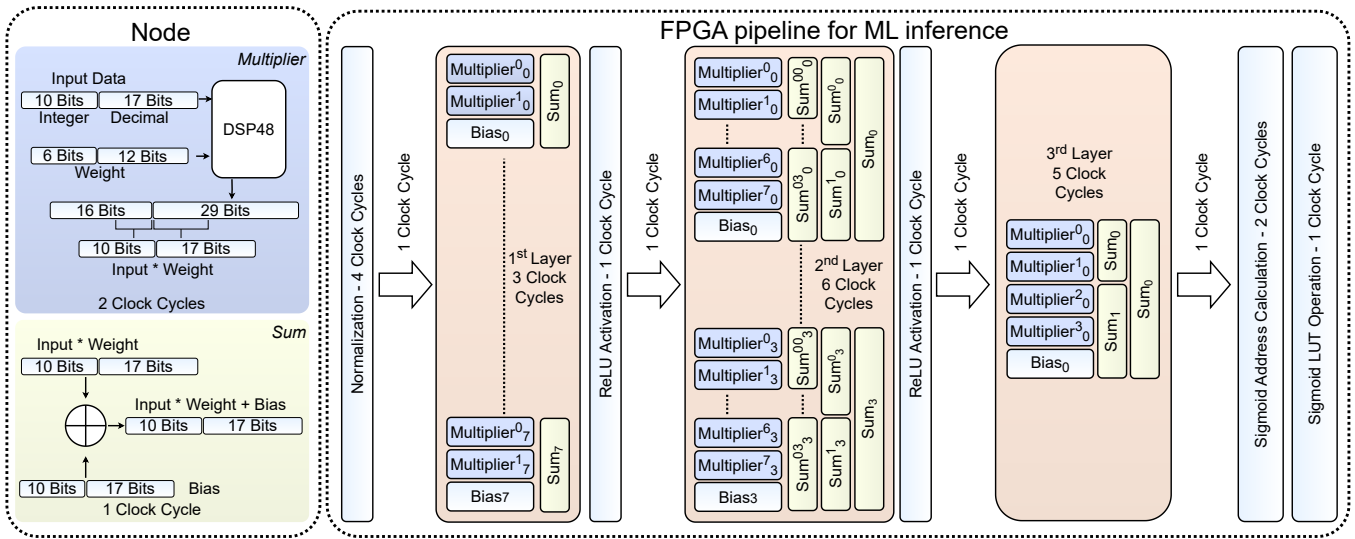


Figure 6: FPGA Pipeline.

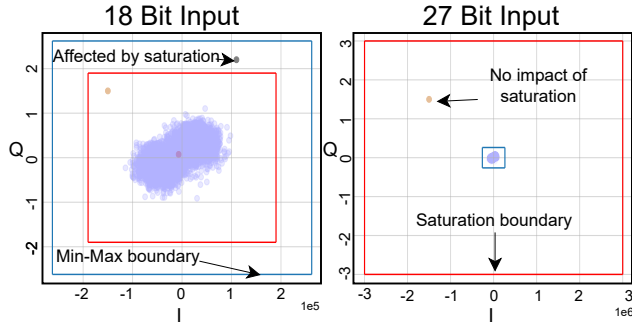


Figure 7: Impact of input width

those operations. For instance, in our setup, where multiplication operations are prevalent, we utilize the Xilinx DSP48 multiplier on FPGA. The DSP48 multiplier accepts operands of 18 bits and 27 bits each and produces a result of 45 bits after multiplication.

As a result, input data to the neural network, i.e., the I and Q data after normalization, are converted into 27-bit fixed-point notation. Within this notation, 10 bits represent the signed integer range  $[-512, 511]$ , and 17 bits represent the decimal range  $[0, 131071]$ . Similarly, biases of the network are converted into 27-bit fixed-point notation. For weights, we use an 18-bit fixed-point notation, with 6 bits reserved for the signed integer range  $[-32, 31]$  and 12 bits for the decimal range  $[0, 4095]$ . This selection of bit widths ensures efficient utilization of resources while maintaining the required precision for neural network computations on FPGA.

After normalization, input data is already confined within the range of  $[0, 1]$  (Figure 8). For instance, let's consider a normalized input value of 0.5454. This value undergoes conversion into a 27-bit fixed-point binary notation, where the integer part is represented by '0' and the decimal part by

'5454'. Consequently, the integer part remains all zeros, denoted as '10b0000000000'. Next, the decimal part is multiplied by  $2^{17}$ , resulting in  $0.5454 * 131072 = 71486$  (ignoring the decimal part). This new number, 71486, is then converted into a 17-bit binary notation, yielding '17b10001011100111110'. Concatenating the integer and binary notations produces '27b000000000010001011100111110', providing the 27-bit fixed-point notation for 0.5454. This procedure is systematically applied to all other parameters and inputs.

Regarding input data from normalization, while the integer part is typically 0 and 1 in rare cases, it could potentially be represented by just 1 unsigned bit. However, using a signed 10-bit integer part is influenced by the subsequent series of multiplication operations that the input undergoes during neural network processing.

As in Figure 7 (left), the blue line represents the min-max boundary, ensuring that every point within the boundary box remains less than  $[1, 1]$  (Post-normalization). Theoretically, data points within this blue box should only require 1 bit for the integer part. However, due to saturation in the later layers of the neural network caused by multiplication operations, points outside the red box may not be correctly classified. Despite being representable within 18-bit precision, some outputs from later layers cannot be accurately represented in this 18-bit notation, resulting in garbage values from that layer onward.

From a series of empirical studies, we confirmed that using a 10-bit integer and 17-bit decimal (total 27-bit) representation mitigates this issue. This choice ensures that the neural network can accurately process the data without encountering saturation-related classification errors.

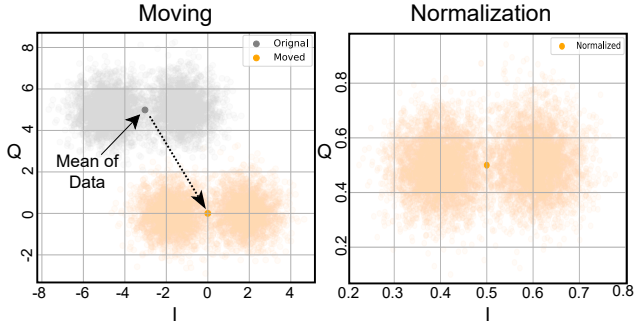


Figure 8: Data scaling

## 6.2 Data scaling on FPGA

Normalization of data before sending it to a neural network is crucial because it ensures consistent scaling across input features, preventing certain features from dominating the learning process due to differences in magnitudes. This stabilizes the training process, accelerates optimization convergence, and enhances the model's generalization ability by reducing sensitivity to input feature scales. While techniques like Z-score or Linear scaling are common in most applications, their implementation on FPGA faces challenges. Most normalization methods require division operations, which demand additional resources and clock cycles, thus becoming a bottleneck for our system. However, FPGA efficiently handles division when the divisor is a power of 2 ( $2^n$ ). Hence, we adapt the linear scaling method to incorporate shifting instead of division, leveraging FPGA's efficiency in performing right shifts for division by powers of 2.

**Moving.** Initially, we adjust the mean of both the I and Q components for the entire dataset to [0,0] (Figure 8). This step ensures that the cluster is evenly distributed across all four Cartesian quadrants, encompassing both positive and negative directions for both I and Q. Such alignment is pivotal for effective normalization implementation.

**Modified normalization.** In linear normalization, as depicted in Equation 5, obtaining the minimum and maximum values of the entire dataset (used for training) is crucial. However, for the division step "max - min", leveraging shifting necessitates converting both the maximum and minimum values to the nearest power of 2. For example, consider the I component of the data (Figure 8), where the maximum is 3000000 and the minimum is -3000000. Utilizing the nearest power of 2, denoted as  $2^{22}$  (4,194,304), for both the min and max values ensures compatibility with the shifting operation.

$$Norm = \frac{X - min}{max - min} \quad (5)$$

It's noteworthy that due to mean shifting, the maximum and minimum values are roughly equivalent but in opposite signs ( $|max| \approx |min|$ ). This detail is significant because if they were significantly different, say the maximum is still 3000000 but

---

### Algorithm 1 Data Scaling

---

- 1:  $data \leftarrow$  input data (scalar)
  - 2:  $n \leftarrow$  nearest  $2^n$  to max of data
  - 3:  $\mu \leftarrow$  mean of data
  - 4:  $tmp \leftarrow (data + 2^n - \mu)$
  - 5:  $data_{norm} \leftarrow ((tmp \ll 17) \gg (n + 1))$
- 

the minimum is -1000000, then the nearest equivalent would be  $2^{21}$ . Consequently, our divisor equation would become  $2^{22} - (-2^{21})$ , which cannot be represented as a power of 2. However, when both maximum and minimum values are approximately equal, such as  $2^{22} - (-2^{22})$  (equivalent to  $2^{23}$ ), we can conveniently employ shift operations for normalization, as illustrated in Equation 6.

$$Norm = (X + 2^n) \gg n + 1 \quad (6)$$

**Decimal representation.** Implementing Equation 6 directly yields all zeros because FPGA does not automatically store data after the decimal point. For instance, consider the I component of the data as 3000000. After normalization, it should ideally be 0.5000, but the equation outputs 0.

$$(a) \quad 3000000 + 2^{22} = 4194352$$

$$(b) \quad 4194352 \gg 23 = 0$$

To address this, we employ a workaround by multiplying numbers by 10,000 before performing the normalization calculation. This ensures that there are 4 digits after the decimal point. Subsequently, the result is multiplied by  $2^{17}$  to convert it into a 17-bit binary representation, as we use 17 bits for decimal representation. Finally, we divide by 10,000 to obtain the desired decimal representation. Here, 65536 represents a 27-bit binary for 0.5000.

$$(a) \quad (3000000 + 2^{22}) * 10000 = 41943520000$$

$$(b) \quad 41943520000 \gg 23 = 5000$$

$$(c) \quad (5000 \ll 17) / 10000 = 65536$$

This process circumvents the need for direct division by 10,000, which FPGA cannot handle efficiently, thus to avoid it we instead multiply and then divide with  $2^{14}$  (16,384). Changing steps as:

$$(a_0) \quad 3000000 + 2^{22} = 4194352$$

$$(a_1) \quad 4194352 \ll 14 = 68720278238$$

$$(b) \quad 68720278238 \gg 23 = 8182$$

$$(c) \quad (8182 \ll 17) \gg 14 = 65536$$

Combining (a<sub>1</sub>), (b), and (c), the final normalization procedure can be obtained. Algorithm 1 shows the entire data scaling procedure, including mean shifting and normalization. This algorithm is applied to I and Q with different values for  $n$ , where  $n$  is precomputed during training. It's important to

note that we use this same data scaling procedure while training to avoid train-test discrepancies.

- (a)  $3000000 + 2^{22} = 4194352$
- (b)  $(4194352 \ll 17) \gg 23 = 65536$

**Finding:** Data representation, which is not an issue in classical computers, turns out to be an important factor in FPGA-based qubit state discrimination. Addressing this issue requires a trade-off between precision and latency.

### 6.3 ML on FPGA

We now discuss the implementation of the model pipeline on the FPGA hardware. We utilized the Xilinx Zynq UltraScale+ RFSoc ZCU216 FPGA [7] for our evaluation, incorporating our system, *QubiCML*. Our main objective is to ensure the hardware performs similarly to its computer-based counterpart with real-time capability.

We adopted a modular approach to implement the FNN architecture, which divides the network into sequences of modules. Each layer, except the input layer, is followed by an activation module and has lists of nodes (neurons). As shown in Figure 6, the node primarily performs multiplication followed by an addition operation. Multiplication operation is always between the weights of the current layer and the output from the previous activation module or input layer. In our architecture, we fixed weights to be 18-bit and input (output of the previous layer) to be 27-bit (Sec. 6.1). Both these operands are input to DSP48 which gives 45-bit output (16-bit integer part, 29-bit decimal part). We use 10 least significant bit (LSB) from the 16-bit integer part and 17 most significant bit (MSB) from the 29-bit decimal part, thus extracting 27-bit (10-bit integer part, 17-bit fraction part) from the 45-bit output for further processing. The output of these digital signal processors (DSP) is added together along with 27-bit bias, as shown in the equation:  $W_0I + W_1Q + B$ .

In our FPGA-based architecture, each multiplication operation is characterized by a duration of 2 clock cycles (4 ns), while addition operations are executed within a single clock cycle (2 ns). Typically, additions involve 2 operands, sourced from DSP outputs, although certain scenarios necessitate 3 operands, including 2 DSP outputs and 1 bias term. To optimize processing efficiency, we enforce a constraint wherein summations are limited to a maximum of 3 operands within a single clock cycle. In cases where more than 3 operands need to be added, we adopt a sequential approach, distributing the summation across that layer, while maintaining parallelism across the node of that layer. For instance, layer 2 has 9 operands (e.g., 8 DSP outputs and 1 bias term) within a single node, a sequential summation strategy is employed

due to the impracticality of executing this operation within 1 clock cycle. Layer 2 operates with 4 such nodes, contributing to a total latency of 6 clock cycles, while layer 3 exhibits a latency of 5 clock cycles.

Layer 1 and 2 within our FPGA architecture are complemented by the ReLU module, a pivotal component characterized by a comparison operation that functions as a threshold on each node of the preceding layer. In essence, the ReLU module determines whether the input from a node is positive or negative: if positive, the output remains unchanged, whereas negative inputs result in an output of 0 for that specific node. The module takes 1 clock cycle.

In the final layer, we employ the sigmoid activation function, a non-linear operation crucial for determining the probability distribution of the qubit states. However, due to its resource-intensive nature on FPGA, we implemented a lookuptable (LUT) approach with predetermined address-value mapping. This involved quantizing the output from layer 3 and utilizing a series of comparison operations to determine the specific address within the LUT, which takes 2 clock cycles. Subsequently, the LUT operation extracts the corresponding value representing the state probability in binary notation, accomplished within a single clock cycle. The entire process, from data normalization to LUT extraction, is executed within 27 clock cycles, translating to 54ns inference time. This streamlined pipeline enables our goal of in-situ real-time qubit state discrimination on the hardware. The output from this pipeline serves as a valuable input for mid-circuit measurement, supporting tasks such as error correction and circuit validation with efficiency and precision.

**Finding:** We successfully designed and implemented a real-time and in-situ ML-powered quantum state discrimination on FPGA hardware.

## 7 EVALUATION

### 7.1 Experimental setup

Our evaluation involved testing with two different QPUs housed in separate dilution fridges, as depicted in Figure 9. One chip featured a TWPA, typically available only in well-established quantum facilities, while the other did not, which was more representative of emerging labs. Each chip contained 8 qubits, resulting in 8 copies of the FNN model within our system, each with unique parameters tailored to different qubits. Additionally, we implemented two types of memory buffers to store model parameters and the state results of experiments.

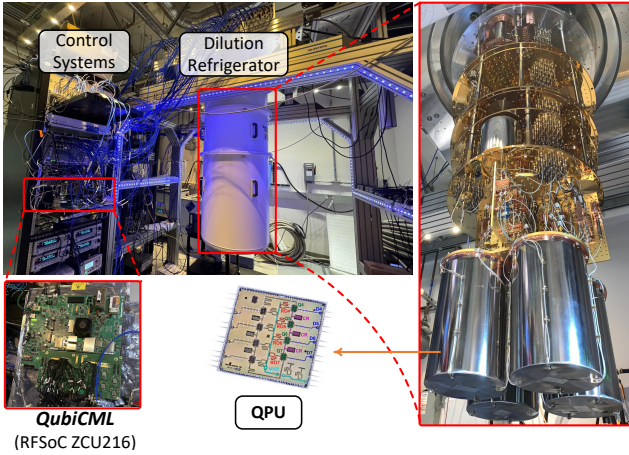


Figure 9: Experimental setup

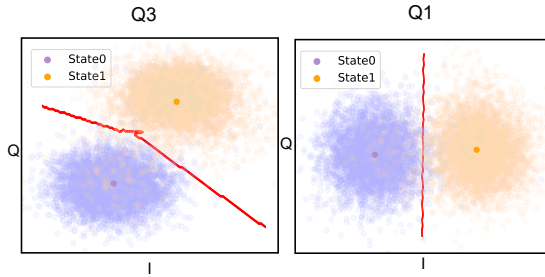


Figure 10: Decision boundary by FNN for 2 qubits without TWPA from QubiCML

Readout Time	Baseline		QubiCML	
	$0 0\rangle$	$1 1\rangle$	$0 0\rangle$	$1 1\rangle$
$2\mu\text{s}$	96.22%	95.81%	99.05%	98.35%
$1.5\mu\text{s}$	92.37%	91.85%	98.76%	98.04%
$1\mu\text{s}$	85.74%	94.66%	95.26%	94.3%

Table 4: Fidelity comparison for qubit Q3.

Readout Time	Baseline		QubiCML	
	$0 0\rangle$	$1 1\rangle$	$0 0\rangle$	$1 1\rangle$
$2\mu\text{s}$	95.85%	95.03%	98.96%	97.88%
$1.5\mu\text{s}$	91.55%	90.87%	98.66%	97.82%
$1\mu\text{s}$	85.05%	84.63%	94.52%	93.24%

Table 5: Fidelity comparison for qubit Q1.

## 7.2 Fidelity across the qubits

**Without TWPA:** While high-fidelity qubit discrimination often requires longer readout times in an environment lacking TWPA due to a low signal-to-noise ratio (SNR), *QubiCML* is still able to make significant fidelity improvements in a reduced timeframe.

Tables 4-5 present our evaluation results on two qubits (without TWPA), specifically Q1 and Q3. Comparing the baseline, which lacks readout envelope optimization, DLO optimization, and utilizes software-based discrimination, *QubiCML*

achieves high fidelity with a relative improvement of 5.07% compared to the baseline for  $1.5\mu\text{s}$ .

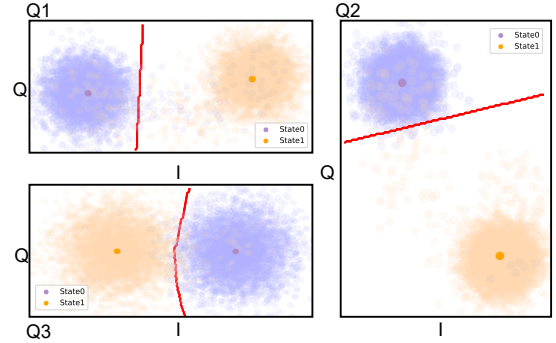


Figure 11: Decision boundary by FNN for 3 qubits with TWPA from QubiCML

**With TWPA:** For the QPU equipped with TWPA, characterized by favorable SNR, achieving high-fidelity qubit state discrimination may occur within shorter readout times. We conducted evaluations on three qubits within a TWPA-equipped fridge.

Qubit	$0 0\rangle$	$1 1\rangle$
Q1 (500ns)	98.82%	98.10%
Q2 (600ns)	98.78%	98.12%
Q3 ( $1\mu\text{s}$ )	97.44%	96.41%

Table 6: *QubiCML* performance evaluated on multiple qubits with TWPA

Table 6 presents our evaluation results for qubits Q1, Q2, and Q3. Remarkably, Q1 achieved a high fidelity of 98.46% with just 500 ns of real-time ML inference, showcasing the system’s capability to rapidly and accurately discriminate qubit states. Similarly, Q2 demonstrated impressive fidelity, achieving 98.42% within a mere 600ns. Conversely, Q3 required a longer readout duration of  $1\mu\text{s}$  to attain high fidelity, emphasizing the variation in readout times among different qubits, which may be influenced by their specific characteristics and interaction dynamics.

Notably, Figure 11 visually illustrates the distinct cluster separation for Q1 and Q2, indicative of shorter required readout times, compared to Q3, which necessitates a longer readout duration to achieve high-fidelity discrimination. This observation underscores the importance of tailoring readout times to the specific characteristics of each qubit to optimize discrimination performance. Moreover, it highlights the effectiveness of *QubiCML* in adapting to and leveraging the favorable SNR conditions provided by TWPA-equipped environments to achieve rapid and accurate qubit discrimination.

### 7.3 Mid-circuit measurement

Mid-circuit measurement plays a crucial role in quantum computing, involving the execution of measurements on specific qubits at predefined intervals during the quantum circuit’s operation. We implemented the FPGA-based real-time state discrimination for a conditional bit-flip mid-circuit measurement. Illustrated in Figure 12, this process entails initializing one qubit (Q2) to a state on the equator, followed by a mid-circuit measurement facilitated by QubiCML’s On-chip FNN pipeline. The outcome of Q2’s mid-circuit measurement determines the subsequent gate operation on another qubit (Q1). For instance, if Q2 yields  $|1\rangle$ , two consecutive X90 gates are applied to Q1; conversely, if Q2 measures  $|0\rangle$ , no operation is performed on Q1. Notably, the final measurement outcome evenly reflects both  $|00\rangle$  and  $|11\rangle$  states, implying the successful implementation of mid-circuit measurement and the feed-forward functionality of the *QubiCML*.

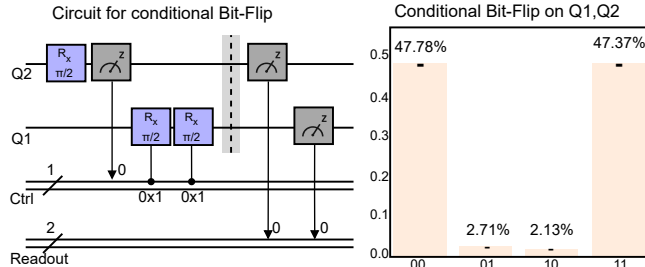


Figure 12: Mid-circuit measurement with *QubiCML* with readout time of 500 ns

### 7.4 Resource usage

Assessing resource utilization is crucial to ensure the efficient operation of the *QubiCML* system on FPGA. Figure 13 provides a detailed overview of resource allocation, highlighting memory allocation for a single ML pipeline in red. To leverage parallelism effectively, we implement 8 ML pipelines, each tailored to the specific parameters of individual qubits. Memory allocation for all 8 qubits is depicted in green, while the allocation by the QubiC system for these qubits is represented in blue/cyan.

Resource allocation is optimized to accommodate the computational demands of *QubiCML*. Table 7 elucidates resource consumption per single qubit, indicating that the majority of resources are utilized for multiplication operations. With our lightweight ML pipeline comprising 52 multiplication operations (52 weights), an equitable distribution of DSPs is necessary to facilitate efficient computation. Moreover, resource utilization for all other operations remains below 0.5%, underscoring the system’s minimal resource footprint.

Resource	Utilization	Utilization %
LUT	1592	0.37%
CARRY8	80	0.15%
FF	2597	0.30%
BRAM	0.5	0.04%
DSP	52	1.11%

Table 7: Resource utilization on Xilinx ZCU216

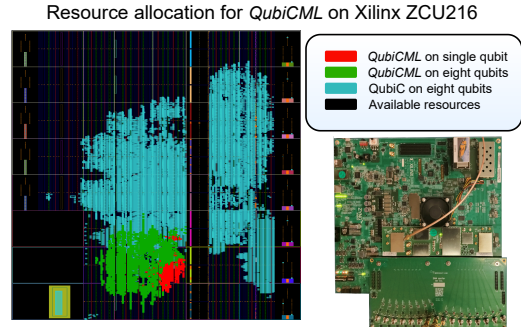


Figure 13: Resource allocation

## 8 RELATED WORK

Recent advancements in qubit discrimination techniques have leveraged developments in both hardware and software, as shown in Table 8. Benjamin et al. introduced a statistical approach utilizing machine learning-based FNNs for multi-qubit readout, but their implementation was hardware-inefficient [25]. Satvik et al. extended this work by introducing optimization techniques like match-filter and relaxed match-filter, leading to a lighter FNN model, but there is no real-time implementation [29]. Hashim et al. demonstrated mid-circuit measurements for active feedback using a single non-statistical approach, highlighting the need for more sophisticated qubit discrimination methods for efficient mid-circuit measurement [17]. Baumer et al. proposed a dynamic decoupling scheme for mid-circuit measurement, but their approach required longer readout times of  $1.2 \mu\text{s}$  with a feed-forward time of  $650 \text{ ns}$ , contrasting with our system’s requirement of just  $54 \text{ ns}$  for feed-forward time [11].

Work	Real-time	Optimization	ML-Based	Mid-Circuit
Benjamin [25]	No	No	Yes	No
Satvik [29]	No	Partially	Yes	No
IBM [11]	Yes	No	No	Yes
Piero [26]	No	No	Yes	No
<b><i>QubiCML</i></b>	<b>Yes</b>	<b>Yes</b>	<b>Yes</b>	<b>Yes</b>

Table 8: Qubit discrimination systems comparison

## 9 CONCLUSIONS & FUTURE WORKS

This paper presents *QubiCML*, an FPGA-based system capable of real-time qubit state discrimination for mid-circuit measurements, an important research milestone in superconducting qubit research. *QubiCML* employs a multi-layer lightweight neural network on an FPGA platform in an efficient manner, achieving accurate in-situ state discrimination with minimal latency. We discuss our important findings obtained from the design and implementation of *QubiCML*. Our evaluation of *QubiCML* demonstrates an average accuracy of 98.5% with only a 500ns shot on three superconducting quantum processors.

## 10 ACKNOWLEDGMENTS

This material is based upon work supported by the U.S. Department of Energy, Office of Science, National Quantum Information Science Research Centers, Quantum Systems Accelerator. Additional support is acknowledged from the U.S. Department of Energy, Office of Science, the Office of High Energy Physics, the National Science Foundation under Award Numbers 2152357 and 2401415, and the Defense Advanced Research Projects Agency under Grant Number HR0011-24-9-0358.

## REFERENCES

- [1] Comprehensive Quantum Feedback and Feed-Forward. <https://www.quantum-machines.co/technology/comprehensive-quantum-feedback-and-feed-forward/>. Accessed: 2024-03-05.
- [2] IBM Quantum Compute Resources. <https://quantum.ibm.com/services/resources?tab=systems>. Accessed: 2024-03-05.
- [3] IBM Unveils Breakthrough 127-Qubit Quantum Processor. <https://newsroom.ibm.com/2021-11-16-IBM-Unveils-Breakthrough-127-Qubit-Quantum-Processor>. Accessed: 2024-03-05.
- [4] Keysight Quantum Control System. <https://www.keysight.com/us/en/products/modular/pxi-products/quantum-control-system.html>. Accessed: 2024-03-05.
- [5] Zurich Instruments Quantum Readout. <https://www.zhinst.com/americas/en/quantum-computing-systems/qubit-readout>. Accessed: 2024-03-05.
- [6] Suppressing quantum errors by scaling a surface code logical qubit. *Nature*, 614(7949):676–681, 2023.
- [7] Advanced Micro Devices, Inc. RFSoc ZCU216. <https://www.xilinx.com/products/boards-and-kits/zcu216.html>, 2024. Accessed: 2024-03-15.
- [8] F. Arute, K. Arya, and et al. Quantum supremacy using a programmable superconducting processor. *Nature*, 574:505–510.
- [9] G. Bebis and M. Georgiopoulos. Feed-forward neural networks. *IEEE Potentials*, 13(4):27–31, 1994.
- [10] C. D. Bruzewicz, J. Chiaverini, R. McConnell, and J. M. Sage. Trapped-ion quantum computing: Progress and challenges. *Applied Physics Reviews*, 6(2):021314, June 2019.
- [11] E. Bäumer, V. Tripathi, A. Seif, D. Lidar, and D. S. Wang. Quantum fourier transform using dynamic circuits. 2024.
- [12] M. E. Deconinck and B. M. Terhal. Qubit state discrimination. *Physical Review A*, 81(6), June 2010.
- [13] M. H. Devoret and R. J. Schoelkopf. Superconducting circuits for quantum information: An outlook. *Science*, 339(6124):1169–1174, 2013.
- [14] K. Fukushima. Cognitron: A self-organizing multilayered neural network. *Biol. Cybern.*, 20(3–4):121–136, sep 1975.
- [15] J. M. Gambetta, J. M. Chow, and M. Steffen. Building logical qubits in a superconducting quantum computing system. *npj Quantum Information*, 3(1), Jan. 2017.
- [16] D. Ha, J. S. Kim, and Y. Kwon. Qubit state discrimination using post-measurement information. *Quantum Information Processing*, 21(2), Jan. 2022.
- [17] A. Hashim, A. Carignan-Dugas, L. Chen, C. Juenger, N. Fruitwala, Y. Xu, G. Huang, J. J. Wallman, and I. Siddiqi. Quasi-probabilistic readout correction of mid-circuit measurements for adaptive feedback via measurement randomized compiling. 2024.
- [18] P. Kalekar. Time series forecasting using holt-winters exponential smoothing. *Time Series Forecasting Using Holt-Winters Exponential Smoothing*, 01 2004.
- [19] N. Kanazawa, H. Emori, and D. C. McKay. Qutrit state discrimination with mid-circuit measurements, Sept. 2023. arXiv:2309.11303 [quant-ph].
- [20] D. P. Kingma and J. Ba. Adam: A method for stochastic optimization, 2017.
- [21] M. Kjaergaard, M. E. Schwartz, J. Braumüller, P. Krantz, J. I.-J. Wang, S. Gustavsson, and W. D. Oliver. Superconducting Qubits: Current State of Play. *Annual Review of Condensed Matter Physics*, 11(1):369–395, Mar. 2020.
- [22] P. Krantz, M. Kjaergaard, F. Yan, T. P. Orlando, S. Gustavsson, and W. D. Oliver. A quantum engineer’s guide to superconducting qubits. *Applied physics reviews*, 6(2), 2019.
- [23] Y. LeCun, Y. Bengio, and G. Hinton. Deep learning. *nature*, 521(7553):436, 2015.
- [24] B. Lienhard, A. Vepsäläinen, L. C. Govia, C. R. Hoffer, J. Y. Qiu, D. Risté, M. Ware, D. Kim, R. Winik, A. Melville, B. Niedzielski, J. Yoder, G. J. Ribeill, T. A. Ohki, H. K. Krovi, T. P. Orlando, S. Gustavsson, and W. D. Oliver. Deep-neural-network discrimination of multiplexed superconducting-qubit states. *Phys. Rev. Appl.*, 17:014024, Jan 2022.
- [25] B. Lienhard and e. a. Vepsäläinen. Deep-neural-network discrimination of multiplexed superconducting-qubit states. *Phys. Rev. Appl.*, 17:014024, Jan 2022.
- [26] P. Luchi, P. E. Trevisanutto, A. Roggero, J. L. DuBois, Y. J. Rosen, F. Turro, V. Amitrano, and F. Pederiva. Enhancing qubit readout with autoencoders. *Physical Review Applied*, 20(1), July 2023.
- [27] C. Macklin, K. O’Brien, D. Hover, M. E. Schwartz, V. Bolkhovskiy, X. Zhang, W. D. Oliver, and I. Siddiqi. A near-quantum-limited josephson traveling-wave parametric amplifier. *Science*, 350(6258):307–310, 2015.
- [28] K. Mannatunga and M. Perera. Performance evaluation of division algorithms in fpga. 01 2016.
- [29] S. Maurya, C. N. Mude, W. D. Oliver, B. Lienhard, and S. Tannu. Scaling qubit readout with hardware efficient machine learning architectures. In *Proceedings of the 50th Annual International Symposium on Computer Architecture*, ISCA ’23, New York, NY, USA, 2023. Association for Computing Machinery.
- [30] C. Neill, P. Roushan, K. Kechedzhi, S. Boixo, S. V. Isakov, V. Smelyanskiy, A. Megrant, B. Chiaro, A. Dunsworth, K. Arya, R. Barends, B. Burkett, Y. Chen, Z. Chen, A. Fowler, B. Foxen, M. Giustina, R. Graff, E. Jeffrey, T. Huang, J. Kelly, P. Klimov, E. Lucero, J. Mutus, M. Neeley, C. Quintana, D. Sank, A. Vainsencher, J. Wenner, T. C. White, H. Neven, and J. M. Martinis. A blueprint for demonstrating quantum supremacy with superconducting qubits. *Science*, 360(6385):195–199, 2018.
- [31] K. Papadantonakis, N. Kapre, S. Chan, and A. Dehon. Pipelining saturated accumulation. 12 2005.

- [32] T. Picot, A. Lupășcu, S. Saito, C. J. P. M. Harmans, and J. E. Mooij. Role of relaxation in the quantum measurement of a superconducting qubit using a nonlinear oscillator. *Phys. Rev. B*, 78:132508, Oct 2008.
- [33] J. Preskill. Quantum Computing in the NISQ era and beyond. *Quantum*, 2:79, Aug. 2018.
- [34] S. Ray and L. Turner. Mahalanobis distance-based two new feature evaluation criteria. *Information sciences*, 60(3):217–245, 1992.
- [35] C. A. Ryan, B. R. Johnson, J. M. Gambetta, J. M. Chow, M. P. da Silva, O. E. Dial, and T. A. Ohki. Tomography via correlation of noisy measurement records. *Physical Review A*, 91(2), Feb. 2015.
- [36] S. Sahin, A. Kavak, Y. Becerkli, and H. Demiray. *Implementation of floating point arithmetics using an FPGA*, pages 445–453. 01 2007.
- [37] E. A. Sete, J. M. Martinis, and A. N. Korotkov. Quantum theory of a bandpass purcell filter for qubit readout. *Phys. Rev. A*, 92:012325, Jul 2015.
- [38] M. S. Shanker, M. Y. Hu, and M. S. Hung. Effect of data standardization on neural network training. *Omega-international Journal of Management Science*, 24:385–397, 1996.
- [39] K. Singh, C. E. Bradley, S. Anand, V. Ramesh, R. White, and H. Bernien. Mid-circuit correction of correlated phase errors using an array of spectator qubits. *Science*, 380(6651):1265–1269, June 2023.
- [40] T. Walter, P. Kurpiers, S. Gasparinetti, P. Magnard, A. Potocnik, Y. Salathe, M. Pechal, M. Mondal, M. Oppliger, C. Eichler, et al. Rapid high-fidelity single-shot dispersive readout of superconducting qubits. *Physical Review Applied*, 7(5):054020, 2017.
- [41] T. Walter, P. Kurpiers, S. Gasparinetti, P. Magnard, A. Potocnik, Y. Salathe, M. Pechal, M. Mondal, M. Oppliger, C. Eichler, and A. Wallraff. Rapid high-fidelity single-shot dispersive readout of superconducting qubits. *Physical review applied*, 7:054020, 2017.
- [42] M. Werninghaus, D. J. Egger, F. Roy, S. Machnes, F. K. Wilhelm, and S. Filipp. Leakage reduction in fast superconducting qubit gates via optimal control. *npj Quantum Information*, 7(1):1–6, Jan. 2021.
- [43] Y. Xu, G. Huang, J. Balewski, R. Naik, A. Morvan, B. Mitchell, K. Nowrouzi, D. I. Santiago, and I. Siddiqi. Qubic: An open-source fpga-based control and measurement system for superconducting quantum information processors. *IEEE Transactions on Quantum Engineering*, 2:1–11, 2021.
- [44] Y. Xu, G. Huang, N. Fruitwala, A. Rajagopala, R. K. Naik, K. Nowrouzi, D. I. Santiago, and I. Siddiqi. Qubic 2.0: An extensible open-source qubit control system capable of mid-circuit measurement and feed-forward. *arXiv preprint arXiv:2309.10333*, 2023.
- [45] Z. Zhang and M. R. Sabuncu. Generalized cross entropy loss for training deep neural networks with noisy labels, 2018.